RSC Advances

ROYAL SOCIETY OF CHEMISTRY

www.rsc.org/advances

Electrochemical sensor based on reduced graphene oxide and copper sulfide hollow nanospheres

Suiping Wang a,b*, Zheng Han a, Yafei Li a, Renfu Peng a, Bo Feng a *

a Department of Food and Biological Engineering, College of Chemical Engineering, Xiangtan University, Xiangtan 411105 China

b State Key Laboratory of Food Science and Technology，Jiangnan University, Wuxi 214122 China

Abstract A nonenzymatic sensor for the detection of hydrogen peroxide (H_2O_2) was fabricated with the reduced graphene oxide (RGO) and the copper sulfide hollow nanospheres (CuSHNs). The RGO was obtained by electrochemical reduction method; and the CuSHNs were acquired using Cu_2O nanoparticles as sacrificial templates. The prepared CuSHNs showed a rough hollow ball structure surrounded with porous shell which supplies many exposed electrocatalytic active sites for the target analyte. The RGO and CuSHNs have good synergistic effects, which can significantly enhance the amperometric response of the sensor toward H_2O_2. Scanning electron microscopy (SEM), transmission electron microscopy (TEM) and electrochemical measurements were used to characterize the RGO and the CuSHNs. The reduction time of graphene oxide, the pH of PBS and applied potential were optimized. Under the optimized experimental conditions, a linear range of 0.005 to 4mM was obtained with the detection limit of 3μM (S/N=3). The linear equation is y=7.1245x+0.3659 (R=0.9989). The reproducibility was investigated with a RSD of 2.46% (*n*=3). The developed

* To whom correspondence should be addressed. Corresponding author, E-mail address: suiping66@126.com. Tel: +86 18873233125

H_2O_2 sensor based on the RGO and CuSHNs possesses advantages such as simple fabrication, fast response, good selectivity, wide linear range and low detection limit.

Keywords Reduced graphene oxide; Copper sulfide hollow nanospheres; Hydrogen peroxide; non-enzymatic sensor

1. Introduction

Graphene is a two-dimensional crystalline sheet of sp^2-hybridized carbon [1] arranged in a honeycombed lattice [2]. It has attracted much attention in the research community owing to the extraordinary properties, such as large surface-to-volume ratio [3-5], superb thermal and electrical conduction [6, 7] and excellent mechanical strength [8]. In recent years, graphene has generated tremendous interest in many fields including catalyst [9, 10], energy storage [11], biosensors [12-14] and so on. The main methods to synthesize graphene including mechanical exfoliation of graphite [15], chemical vapor deposition [16], reduction of graphene oxide (GO) [17]. Scientists have developed several methods for GO reduction, such as high-temperature annealing in vacuum or noble gases, chemical reduction in aqueous solution and eletrochemial reduction [18].

Hollow nanospheres have been recently attracted enormous attention owing to unique performance, and have been applied in many fields including drug delivery [19], catalysts [20], sensors [21, 22] and artificial cell [23]. The synthetic strategies for hollow structures include hard-templating and soft-templating methods, sacrificial

templating, Kirkendall effect and Ostwald ripening [24-27]. Hollow metallic nanoballs exhibit unique adsorption and catalytic properties different from their solid counterparts, with the advantage of low density, high specific surface, and reduction of costs. To the best of our knowledge, the hollow structure in the application of non-enzymatic electrochemical sensor is increasing [28-30].

Copper sulfide (CuS) is an important semiconductor material with unique electronic, optical, chemical and physical properties, which has potential applications in sensors [22, 31], catalysts [32], and solar cells [33]. In this work, CuS hollow nanospheres (CuSHNs) have been simply synthesized using Cu_2O spheres as sacrificial templates. The electrochemical reduction has been chosen to prepare graphene. An electrochemical non-enzymatic sensor fabricated with the RGO and CuSHNs has been demonstrated. The RGO and CuSHNs have good synergistic effects, which can significantly enhance the amperometric responses of the sensor toward H_2O_2.

2. Experimental

2.1 Reagents and apparatus

Graphite powders, $Na_2HPO_4 \cdot 12H_2O$, $NaH_2PO_4 \cdot 2H_2O$, $Na_2S \cdot 9H_2O$, $Cu(NO_3)_2 \cdot 3H_2O$, KCl, $NaNO_3$, polyvinylpyrrolidone (PVP), hydrogen peroxide (H_2O_2), β-D-glucose, ascorbic acid (AA), dopamine (DA) were purchased from Sinopharm Group Chemical Reagent Co, Ltd. (Shanghai, China). Phosphate buffer solutions (PBS) with various pH were prepared by mixing suitable 0.1M NaH_2PO_4/Na_2HPO_4. All other reagents were of analytical reagent grade and used as

received without further purification. Ultrapure water was used throughout with a resistance of 18.25 MΩ·cm. Before each electrochemical measurement, solutions were saturated with N_2 by bubbling N_2 through the solution for at least 20 min to remove dissolved O_2.

All electrochemical measurements were performed in a conventional three electrode system with the modified GCE as the working electrode, a saturated calomel electrode (SCE) as reference electrode and a platinum electrode as counter electrode. All potentials reported were versus the SCE and all experiments were carried out at room temperature. Scanning electron microscopy (SEM) analysis was performed using a JSM-6610LV microscope (JEOL, Ltd., Japan). Transmission electron microscopy (TEM) analysis was performed using a Titan G2 60-300 microscope with image corrector (FEI, Ltd., USA). Cyclic voltammetry and amperometric measurements were carried out on CHI 660D electrochemical workstation (Shanghai CH Instruments Co., China). Raman scattering was performed on Renishaw InVia Raman microscope, using a 532 nm laser source. The Powder X-ray diffraction (XRD) measurements were performed on a D/max2550 18KW rotating anode X-ray diffractometer with monochromatic Cu Kα radiation (λ = 1.5418 Å) at a voltage and current of 40 kV and 300 mA.

2.2. Preparation of graphene oxide (GO)

Prior to experiment，all glassware used were thoroughly cleaned with freshly aqua regia and then rinsed repeatedly with ultrapure water before use. GO was prepared using a modified Hummers and Offeman's method [34]. Briefly, 0.5g of

graphite powders, 0.5g of $NaNO_3$ and 23mL of H_2SO_4 were stirred together in an ice bath. Then, 3g of $KMnO_4$ was slowly added. After mixed, the solution was transferred to a 35 ^oC water bath and stirred for 1h, forming a thick paste. Next, 40mL of water was added, and the solution was stirred for 30min at the temperature of 95 ^oC. Finally, 100mL of water was added, followed by the slow addition of 3mL of H_2O_2 (30%), turning the color of the solution from dark brown to yellow. Firstly, the obtained solution underwent low-speed centrifugation at 1000rpm for 2min. The centrifugation was repeated about 3-5 times until all visible particles were removed. Then the supernatant went through two high-speed centrifugation steps at 8000 rpm for 15 min to remove small GO pieces and water-soluble byproduct. The obtained sediment was washed with 100mL 10% HCl (w/w) by centrifugation, and subsequently washed with ultrapure water until the solution was neutral. The final sediment was vacuum-dried over 24 h at 50 ^oC. The synthesized moderate solid product was redispersed in water with mild sonication using a table-top ultrasonic cleaner for ultrasonic stripping (2h), giving a solution of exfoliated GO with a concentration of 0.5mg/mL.

2.3. Synthesis of CuS hollow nanospheres

CuS hollow nanospheres were synthesized according to previously reported method with slight modifications [19, 35]. In a typical protocol, $Cu(NO_3)_2$ solution (100μL, 0.5M) was added to ultrapure water (25mL) containing polyvinylpyrrolidone (PVP, 0.24g) in a round-bottom flask under magnetic stirring for 20min at room temperature. Then, NaOH solution (25mL, pH 9.0) was added, followed by addition of hydrazine hydrate solution (8μL, 80%w/w) to form a suspension of Cu_2O spheres.

After 5min, Na_2S aqueous solution (200μL, 320mg/mL) was added into the suspension. The obtained solution was heated at 60 ^oC for 3h with reflux under magnetic stirring in water bath. The product was centrifuged thrice at 8,000rpm for 10min to remove impurities. After centrifugation and washing, the as-purified CuS hollow nanospheres were dispersed well in water.

2.4. Fabrication of the H_2O_2 sensor

The fabrication procedure of the GCE by the CuSHNs and RGO (CuSHNs/RGO/GCE) is illustrated schematically in Scheme 1. A bare GCE with diameter of 2 mm was carefully polished with 0.05μm α-Al_2O_3 power slurry to obtain a mirror shiny surface, and successively rinsed thoroughly with absolute alcohol and ultrapure water in ultrasound bath for 3min. After that, 8μL of 0.5mg/mL GO solution was dropped onto the surface of the pretreated GCE and left to dry at room temperature to get GO-modified GCE. The electrochemical reduction of exfoliated GO was performed at -1.3V (vs SCE) in 0.5M NaCl solution for 300s by chronoamperometry [36, 37]. The obtained reduced graphene oxide modified GCE was referred as RGO/GCE. Subsequently, 5μL of CuS hollow nanospheres was cast onto the RGO/GCE surface and left to dry at room temperature to obtain CuSHNs/RGO/GCE. For comparison, the CuS hollow nanospheres-modified GCE (CuSHNs/GCE) was prepared in the same way.

3. Results and discussion

3.1. Characterization of the reduced graphene oxide (RGO), Cu_2O template and CuS hollow sphere

A typical scanning electron microscope (SEM) image of RGO formed is presented in Figure 1A. It is observed that the RGO presented a typical flake-like shape with slight wrinkles on the surface, as reported previously [38]. Figure 1B is the SEM image of Cu_2O spheres, showing that the Cu_2O nanoparticles are of regular spheres with uniform morphology, and the average diameter of spheres is 130nm.

The detailed preparation and growth mechanism of CuSHNs have been described elsewhere [35]. The sacrificial template chemical transformation method based on the Kirkendall effect has been demonstrated to be an effective approach. In this method, the sacrificial templates transform to the aimed at shell through chemical reaction on the templates' surface, and the core is removed by Kirkendall diffusion at the same time, and therefore no modification of the template surface and no special process for removing the template core are needed. Briefly, the Cu_2O spheres, served as sacrificial template, when Na_2S was added into the Cu_2O suspension (in order to bring sulfurization treatment) and hollow nanostructure with shell is formed. As shown in the low-magnification TEM image (Fig.1C), the hollow structure is well-produced through sulfurizing procedure. S^{2-} released from the ionization of Na_2S reacts with the Cu_2O nanoparticles on the spheres' surface to generate CuS nanoparticles. With further reaction, the CuS nanoparticles are formed on the outside and inside surfaces of the CuS shell. Finally, the hollow shell appeared instead of initial solid Cu_2O sphere. The following reactions may be involved:

$$4Cu^{2+}+8OH^{-}+N_2H_4\cdot H_2O=2Cu_2O+7H_2O+N_2 \quad (1)$$

$$2Cu_2O+4S^{2-}+O_2+4H_2O=4CuS+8OH^{-} \quad (2)$$

The transmission electron microscopy (TEM) images show that the CuS hollow nanospheres are hollow structures with an average outer diameter of around 150nm and the thickness of shell is about 25nm (Fig.1 C, D). The strong contrast between the edge and centre parts provides convincing evidence for its hollow nature. The prepared CuSHNs showed a rough hollow ball structure surrounded with dense CuS nanocrystallites which can increase electrocatalytic active sites for H_2O_2.

Raman spectroscopy is an effective tool to measure the structural change of GO after reduction. Figure 2 shows the Raman spectra of GO and RGO. It is seen that both spectra exhibit two characteristic main peaks: the D band at ~1350 cm^{-1}, and the G band at ~1600 cm^{-1}. However, the intensity ratio of D/G increased after the electrochemical reduction, which means that GO was reduced and RGO was obtained [18, 36, 37]. Figure 3A shows the XRD pattern of the Cu2O templates. All diffraction peaks in the pattern can be indexed to the pure cubic phase of Cu2O (JCPD file No. 77-0199). Figure 3B shows the XRD pattern of the obtained CuS hollow nanospheres . It can be seen that all peaks in the pattern can be indexed to hexagonal covellite CuS (JCPD file No. 06-0464) [35].

3.2. Electrochemical characterization of the modified electrode

The electrochemical performances of the different modified GCEs in 5mM $K_3[Fe(CN)_6]/K_4[Fe(CN)_6]$ containing 0.1M KCl at a scan rate of 100mV/s were presented in Fig.4A. As we can see from Fig.4A, when exfoliated GO is modified

onto a GCE surface, the redox peak current significantly decreases as compared to the bare GCE, suggesting that the exfoliated GO acts as an insulating layer which makes the interfacial charge transfer difficult and the surface charges of the exfoliated GO repel the access of ferricyanide and ferrocyanide ions to the electrode surface for electron communication as well [36, 37]. After the exfoliated GO is electrochemically reduced on the electrode at -1.3V, the redox peak current increases distinctively, indicating that RGO has accelerated electron transfer between the electrochemical probe $[Fe(CN)_6]^{3-/4-}$ and the electrode. The main reason is attributed to dramatically improved electrical conductivity of the RGO. Fig.4B shows the cyclic voltammograms (CVs) of bare GCE, RGO/GCE, and CuSHNs/RGO/GCE in 0.1M PBS (pH=7.0). It is clearly seen that the CVs of bare GCE or RGO/GCE only show glossy tracks, indicating no electroactive substance exist on the electrode surface. The CV of RGO/GCE shows higher background current than that of bare GCE owing to the increase of the electrode surface and the excellent electrical conduction of RGO. Compared with bare GCE and RGO/GCE, a pair of redox peaks appeared at−260mV and −100mV of the CuSHNs/RGO/GCE (curve c) in the blank PBS, which might be attributed to the Cu_2S/CuS redox couple, similar to previous report [31]. Their hollow architecture promotes analyte diffusion and increases the available active surface area.

The amperometric responses of the different modified electrodes upon successive additions of H_2O_2 at an applied potential of −100mV were shown in Fig.5. It can be obviously found that the RGO and CuSHNs modified glassy carbon electrode (CuSHNs/RGO/GCE, curve c) have the largest current response toward

H_2O_2 sensing. The current responses (curve c, 11.2μA) are much larger than the sum of CuSHNs modified GCE (curve b, 3.8μA) and RGO modified GCE (curve a, 2.4μA). The results show that RGO and CuSHNs maybe have good synergistic effect, which indicates the porous shell of CuS hollow nanosphere supplies many exposed electrocatalytic active sites for the H_2O_2 reduction and provide high electron transfer rate by an efficient electrical network through CuSHNs direct anchoring on the surface of RGO.

Fig.6 shows the CVs of CuSHNs/RGO/GCE in the absence (a) and presence (b) of 1mM H_2O_2 in the N_2-saturated 0.1M PBS (pH=7.0) at a scan rate of 100mV/s. In the absence of H_2O_2, CuSHNs/RGO/GCE displayed a pair of oxidative and reductive peaks in the potential range from −600 to +100mV, which might be attributed to the reduction of CuS to Cu_2S and the reoxidation of Cu_2S back to CuS. Upon addition of 1mM H_2O_2, the reduction peak current increased significantly, and the oxidation peak current decreased obviously. These results suggest that the CuSHNs/RGO/GCE possesses excellent electrocatalytic activity toward the reduction of H_2O_2. Such excellent catalytic activity of CuSHNs/RGO/GCE may be attributed to the synergistic effect between RGO and CuSHNs. The CuS hollow architecture promotes analyte diffusion and increases the available active surface area.

3.3. Optimization of the electrochemical measurement

Fig.7A displays the effect of the different electrochemical reduction time of graphene oxide on the amperometric response of CuSHNs/RGO/GCE toward 2mM H_2O_2. It can be seen that the current response increases with the enhancement of the

reduction time, reaching the maximum value at 300s, and then suffers a slight decrease when the reduction time was further increased. Thus, the reduction time of 300s was chosen as the optimized condition. The effect of pH on the amperometric response of CuSHNs/RGO/GCE toward 2mM H_2O_2 was also investigated, as shown in Fig.7B. It can be seen that the maximum current response appear at pH 7.0. Thus, we select PBS of pH 7.0 as the supporting electrolyte in this work. The amperometric responses of the sensor towards constant H_2O_2 concentration (2mM) with applied potential in the range from 500mV to -500mV is shown in Fig.7C. As can be seen, when the applied potential was from 0 to -500mV, the maximum response current appear at -300mV. When the potential was more positive than 0V, the current response is very slight. The results suggest that the reduction of H_2O_2 was easily achieved at low negative potential. Thus, -300mV was finally selected.

3.4. Analytical performance of the sensor

The typical i-t curves of the CuSHNs/RGO/GCE on the successive addition 1 mM H_2O_2 under the optimized experimental conditions are displayed in Fig.8A. As can be seen, the sensor could achieve the maximum steady-state current within 3s. Fig.8B shows the calibration curve of the amperometric responses versus H_2O_2 concentrations under the optimized conditions. The linear detection range was from 0.005 to 4mM with a correlation coefficient of 0.9989. The detection limit was estimated to be 3μM at the signal-to-noise ratio of 3. The obtained analytical parameters are compared with that of the previously reported H_2O_2 sensors, which are listed in Table 1 [31, 39-47].

From Table 1, one can see that the proposed sensor in this work presents a relatively low detection limit and a relatively wide linear range in comparison with some other electrochemical H_2O_2 sensors. It reveals the excellent performance of CuSHNs/RGO/GCE. It owes to the synergistic effect between CuSHNs and RGO, which could enhance the catalytic ability of the sensor. The developed electrochemical sensor shows excellent sensing properties towards H_2O_2, including fast response rate, wide linear range and low detection limit.

3.5. Selectivity, repeatability and reproducibility of the H_2O_2 sensor

The selectivity is one of the most important analytical factors for a sensor. In this work, we select dopamine (DA) and ascorbic acid (AA) as interfering substances in order to investigate the selectivity of this non-enzymatic sensor. As shown in Fig.9, there was obvious current response to the addition of 1.3 mM H_2O_2. However, there were no significant current changes after the addition of the electroactive species DA, and AA. We can conclude that the above species cause negligible effect for the H_2O_2 sensing and the proposed sensor has a superior selectivity towards H_2O_2.

The repeatability and reproducibility of the fabricated sensor was also investigated. The relative standard deviation (RSD) of the current response to 2mM H_2O_2 was 2.27% for three successive measurements. Three sensors fabricated independently give a RSD of 2.46%. These results indicate that the proposed sensor had an acceptable repeatability and good reproducibility.

4. Conclusion

In this paper, a non-enzymatic H_2O_2 sensor based on the RGO and CuSHNs was

developed. We proposed a simple and low-power consumption electrochemical method to prepare reduced graphene oxide sheets. The prepared CuSHNs showed a rough hollow ball structure surrounded with dense CuS nanocrystallites which can increase electrocatalytic active sites for H_2O_2. Their hollow architecture promotes analyte diffusion and increases the available active surface area. The RGO and CuSHNs have good synergistic effects, which can significantly enhance the electrocatalytic performance of the sensor toward H_2O_2. The electrochemical sensor based on the RGO and CuSHNs exhibited fast response, wide linear range, low detection limit and good selectivity. The CuSHNs/RGO can be served as a promising platform for electrochemical sensors.

Acknowledgements

This work was supported by the National Natural Science Foundation of China (31401577, 31270988)，Hunan Provincial Natural Science Foundation of China (13JJ9004), the Open Project Program of State Key Laboratory of Food Science and Technology，Jiangnan University (SKLF-KF-201107), Scientific Research Foundation for Doctors of Xiangtan University (11QDZ04).

References

[1] M.J. Allen, V.C. Tung and R.B. Kaner, *Chem. Rev.,* 2010, **110**, 132-145.

[2] S.Y. Kwon, C.V. Ciobanu, V. Petrova, V.B. Shenoy, J. Bareño, V. Gambin, I. Petrov and S. Kodambaka, *Nano Lett.,* 2009, **9**, 3985-3990.

[3] S.J. Park and R.S. Ruoff, *Nat. Nanotech,.* 2009, **4**, 217-224.

[4] A.K. Geim and K.S. Novoselov, *Nat. Mater.,* 2007, **6**, 183-191.

[5] M.D. Stoller, S.J. Park, Y.W. Zhu, J.H. An and R.S. Ruoff, *Nano Lett.,* 2008, **8**, 3498-3520.

[6] A.A. Balandin, S. Ghosh, W.Z. Bao, I. Calizo, D. Teweldebrhan, F. Miao and C.N. Lau, *Nano Lett*., 2008, **8**, 902-907.

[7] K.I. Bolotin, K.J. Sikes, Z. Jiang, M. Klima, G. Fudenberg, J. Hone, P. Kim and H.L. Stormer, *Solid State Commun*., 2008, **146**, 351-355.

[8] C.G. Lee, X.D. Wei, J.W. Kysar and J. Hone, *Science,* 2008, **321**, 385-388.

[9] X J Bai, L Wang, R L Zong, Y.H. Lv, Y.Q. Sun and Y.F. Zhu, *Langmuir,* 2013, **29***,* 3097-3105.

[10] B. Weng, J. Wu, N. Zhang and Y.J. Xu, *Langmuir,* 2014, **30**, 5574-5584.

[11] W. Lv, D.M. Tang, Y.B. He, C.H. You, Z.Q. Shi, X.C. Chen, C.M. Chen, P.X. Hou, C. Liu and Q.H. Yang, *ACS Nano,* 2009, **3**, 3730-3736.

[12] D. Chen, L.H. Tang and J.H. Li, *Chem. Soc. Rev.,* 2010, **39**, 3157-3180.

[13] S.J. Guo and S.J. Dong, *Chem. Soc. Rev.,* 2011, **40**, 2644-2672.

[14] F.G. Xu, Y.J. Sun, Y. Zhang, Y. Shi, Z.W. Wen and Z. Li, *Electrochem.*

Commun., 2011, **13**, 1131-1134.

[15] K.S. Novoselov, A.K. Geim, S.V. Morozov, D. Jiang, Y. Zhang, S.V. Dubonos, I.V. Grigorieva and A.A. Firsov, *Science,* 2004, **306**, 666-669.

[16] K.S. Kim, Y. Zhao, H. Jang, S.Y. Lee, J.M. Kim, K.S. Kim, J.H. Ahn, P. Kim, J.Y. Choi and B.H. Hong, *Nature,* 2009, **457**, 706-710.

[17] D. Li, M.B. Müller, S. Gilje, R.B. Kaner and G.G. Wallace, *Nat. nanotech*., 2008, **3***,* 101-105.

[18] Y.L. Guo, B. Wu, H.T. Liu, Y.Q. Ma, Y. Yang , J. Zheng, G. Yu and Y.Q. Liu, *Adv. Mater*., 2011, **23**, 4626-4630.

[19] S. Ramadan, L.R. Guo, Y.J. Li, B.F. Yan and W. Lu, *small,* 2012, **8**, 3143-3150.

[20] S.W. Kim, M. Kim, W.Y. Lee and T. Hyeon, *J. Am. Chem. Soc*., 2002, **124**, 7642-7643.

[21] S.F. Liu, J. Liu, X.P. Han, Y.N. Cui and W. Wang, *Biosens. Bioelectron.,* 2010, **25**, 1640-1645.

[22] X.L. Yu, Y. Wang, H.L.W. Chan and C.B. Cao, *Microporous Mesoporous Mater*., 2009, **118**, 423-426.

[23] T.K. Maji, R. Matsuda and S. Kitagawa, *Nat. Mater*., 2007, **6**, 142-148.

[24] L.M. Qi, J. Li and J.M. Ma, *Adv. Mater*., 2002, **14**, 300.

[25] H. J. Fan, U. Gösele and M. Zacharias, *small,* 2007, **3**, 1660-1671.

[26] H.C. Zeng, *J. Mater. Chem*., 2006, **16**, 649-662.

[27] X.W. Lou, L.A. Archer and Z.C. Yang, *Adv. Mater*., 2008, **20**, 3987-4019.

[28] G. Nie, X. Lu, J. Lei, L. Yang, X. Bian, Y. Tong and C. Wang, *Electrochimica*

Acta, 2013, **99**, 145-151.

[29] L. Tian, X. Zhong, W. Hu, B. Liu and Y. Li, *Nanoscale Research Letters*, 2014, **9**, 68-72.

[30] A. J. Wang, J. J. Feng, Z. H. Li, Q. C. Liao, Z. Z. Wang and J. R. Chen, *CrystEngComm*, 2012, **14**, 1289-1295.

[31] J. Bai and X.E. Jiang, *Anal. Chem*., 2013, **85**, 8095-8101.

[32] M. Basu, A.K. Sinha, M. Pradhan, S. Sarkar, Y. Negishi, Govind and T. Pal, *Environ. Sci. Technol*., 2010, **44**, 6313-6318.

[33] K.D. Yuan, J.J. Wu, M.L. Liu, L.L. Zhang, F.F. Xu, L.D. Chen and F.Q. Huang, *Appl. Phys. Lett*. 2008, **93**, 1.

[34] L.J. Cote, F. Kim and J.X. Huang, *J. Am. Chem. Soc*., 2009, **131**, 1043-1049.

[35] H.T. Zhu, J.X. Wang and D.X. Wu, *Inorg. Chem*., 2009, **48**, 7099-7104.

[36] H.L. Guo, X.F. Wang, Q.Y. Qian, F.B. Wang and X.H. Xia, *ACS Nano,* 2009, **3**, 2653-2659.

[37] Z.J. Wang, X.Z. Zhou, J. Zhang, F. Boey and H. Zhang, *J. Phys. Chem. C,* 2009, **113**, 14071-14075.

[38] A.K. GEIM, *Science,* 2009**, 324**, 1530-1534.

[39] J.G. Hu, F.H. Li, K.K. Wang, D.X. Han, Q.X. Zhang, J.H. Yuan and L. Niu, *Talanta,* 2012, **93**, 345-349.

[40] F.H. Meng, X.L. Yan, J.G. Liu, J. Gu and Z.G. Zou, *Electrochim. Acta,* 2011, **56**, 4657-4662.

[41] S. Liu, J.Q. Tian, L. Wang, H.L. Li, Y.W. Zhang and X.P. Sun, *Macromolecules,*

2010, **43**, 10078-10083.

[42] W.B. Lu, F. Liao, Y.L. Luo, G.H. Chang and X.P. Sun, *Electrochim. Acta,* 2011, **56**, 2295-2298.

[43] X.H. Niu, H.L. Zhao, C. Chen and M.B. Lan, *Electrochim. Acta,* 2012, **65**, 97-103.

[44] Y.P. Ye, T. Kong, X.F. Yu, Y.K. Wu, K. Zhang and X.P. Wang, *Talanta,* 2012, **89**, 417-421.

[45] A.K. Dutta, S. Das, P.K. Samanta, S. Roy, B. Adhikary and P. Biswas, *Electrochim. Acta,* 2014, **144**, 282-287.

[46] L. Zhang, Y.H. Ni, X.H. Wang and G.C. Zhao, *Talanta,* 2010, **82**, 196-201.

[47] C.X. Lei, H. Wang, G.L. Shen and R.Q. Yu, *Electroanal.* 2004, **16**, 736-740.

Captions of Figures:

Scheme 1 Schematic illustration of the stepwise modification of the CuSHNs/RGO/GCE sensor.

Table 1 Comparison of various H_2O_2 sensors using chemically modified electrode

Fig.1 (A, B) SEM images of the reduced graphene oxide and Cu_2O spheres; (C, D) TEM images of the CuS hollow nanospheres.

Fig.2 Raman spectra of GO (A) and RGO (B).

Fig. 3 XRD diffractograms of Cu_2O (A) and CuS (B)

Fig. 4 (A) Cyclic voltammetry of bare GCE (a), GO/GCE (b) and RGO/GCE (c) in 5mM $K_3[Fe(CN)_6]/K_4[Fe(CN)_6]$ containing 0.1M KCl; (B) Cyclic voltammetry of the bare GCE (a), RGO/GCE (b) and CuSHNs/RGO/GCE (c) in 0.1M PBS (pH=7.0).

Fig. 5 Amperometric responses of the RGO/GCE (a), CuSHNs/GCE (b) and CuSHNs/RGO/GCE (c) to successive additions of 2mM H_2O_2 into 0.1M PBS (pH=7.0) at -100mV.

Fig. 6 CVs of CuSHNs/RGO/GCE in N_2-saturated 0.1 M PBS (pH=7.0) in the absence (a) and presence (b) of 1mM H_2O_2 at a scan rate of 100mV/s.

Fig. 7 Effects of the reduction time of GO (A) and pH value of PBS (B) on the amperometric responses of CuSHNs/RGO/GCE toward 2mM H_2O_2 at -100mV; effect of the applied potential (C) on the amperometric responses of CuSHNs/RGO/GCE toward 2mM H_2O_2.

Fig. 8 (A) Amperometric responses of HCuSPs/RGO/GCE on successive injection of 1.0mM H_2O_2 into 0.1M PBS (pH=7.0) at the applied potential of -300mV; (B) The

calibration plot of the amperometric responses versus the H_2O_2 concentration under the optimized conditions. Applied potential: -300mV.

Fig.9 Amperometric responses of CuSHNs/RGO/GCE upon the successive additions of 1.3 mM H_2O_2, dopamine (DA) and ascorbic acid (AA) into N_2-saturated 0.1M PBS (pH=7.0) under a stirring condition. Applied potential: −300mV.

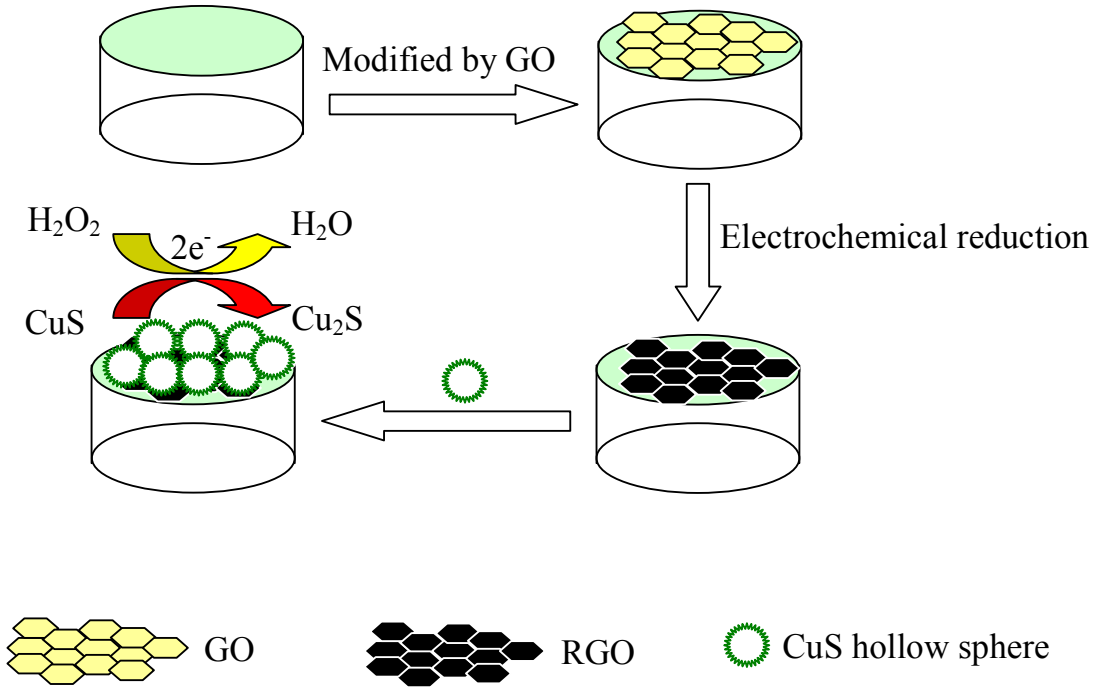

Scheme 1 Schematic illustration of the stepwise modification of the CuSHNs/RGO/GCE sensor.

Table 1 Comparison of various H_2O_2 sensors using chemically modified electrode

Electrode	Linear range (mM)	Detection limit (μM)	References
CuS-RGO composite/GCE	0.005-1.5	0.27	[30]
Graphene-AuNPs[a]/GCE	0.02-0.28	6.0	[39]
NPG[b]/GCE	0.01-8.0	3.26	[40]
Graphene-AgNPs[c]/GCE	0.1-40	28.0	[41]
PQ11[d]-AgNPs/GCE	0.1-180	33.9	[42]
SPGFE[e]/MWCNTC[f]/PtNP[g]	0.005-2.0	1.23	[43]
Fe_3O_4-RGO composite/Au electrode	0.1-6.0	3.2	[44]
CuSNPs[h]/GCE	0.01-1.9	1.1	[45]
α-Fe_2O_3-CH[i]/GCE	0.001-0.044	0.4	[46]
HRP[j]/nano-Au film/GCE	0.0061-1.8	6.1	[47]
CuSHNs/RGO/GCE	0.005-4.0	3.0	This work

[a] Au nanoparticles
[b] Nanoporous gold
[c] Ag nanoparticles
[d] Poly[(2-ethyldimethylammonioethyl methacrylate ethyl sulfate)-co-(1-vinylpyrrolidone)]
[e] Screen-printed gold film electrode
[f] Multi-walled carbon nanotube clusters
[g] Platinum nanoparticles
[h] CuS nanoparticles
[i] Chitosan
[j] Horseradish peroxidase

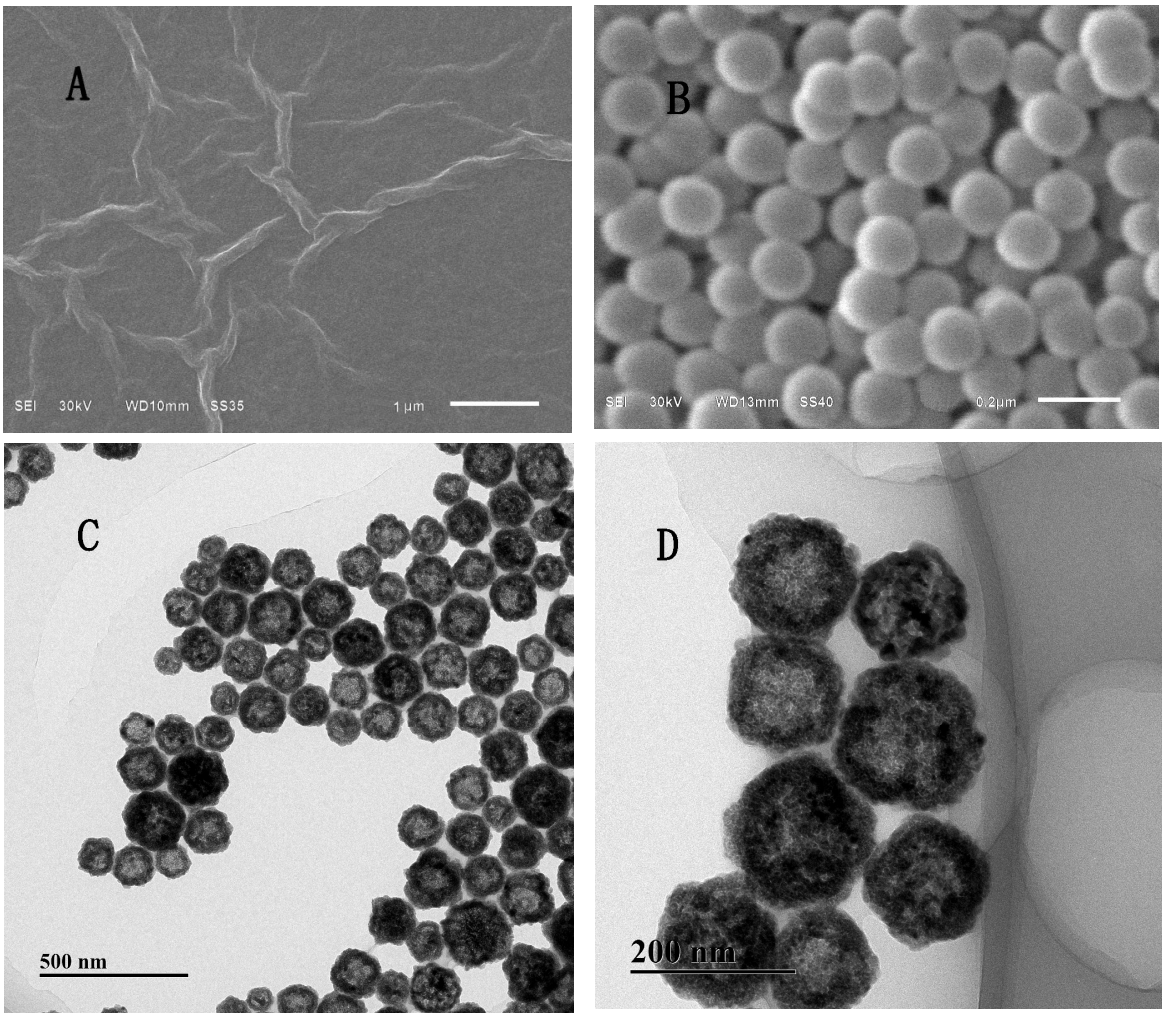

Fig.1 (A, B) SEM images of the reduced graphene oxide and Cu_2O spheres; (C, D) TEM images of the CuS hollow nanospheres.

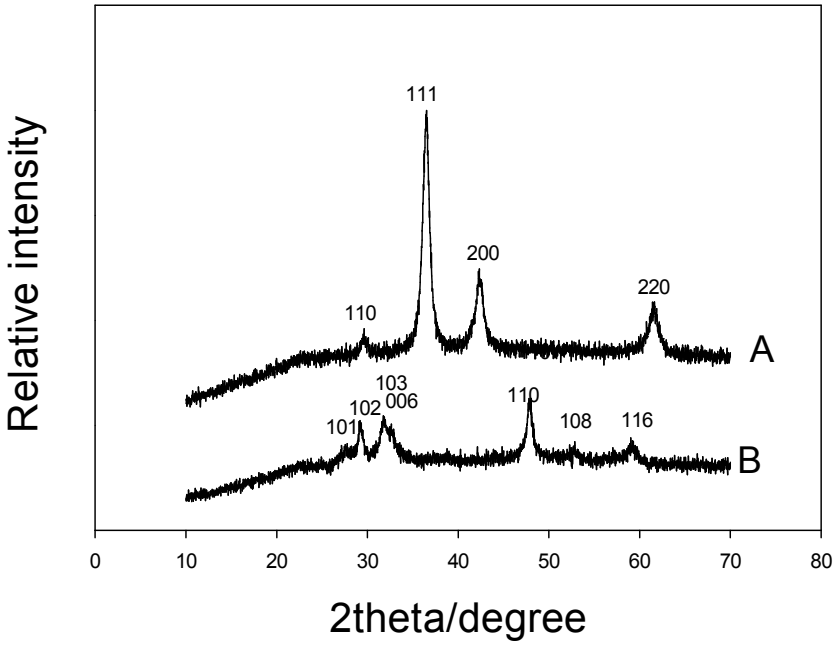

Fig.2 Raman spectra of GO (A) and RGO (B).

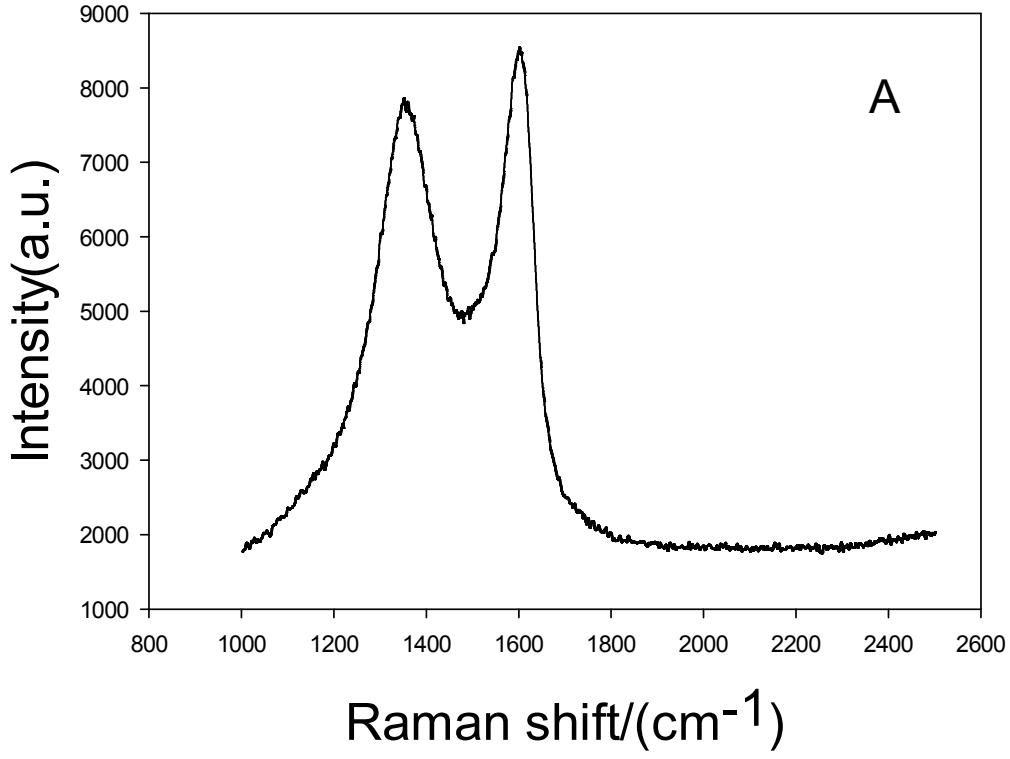

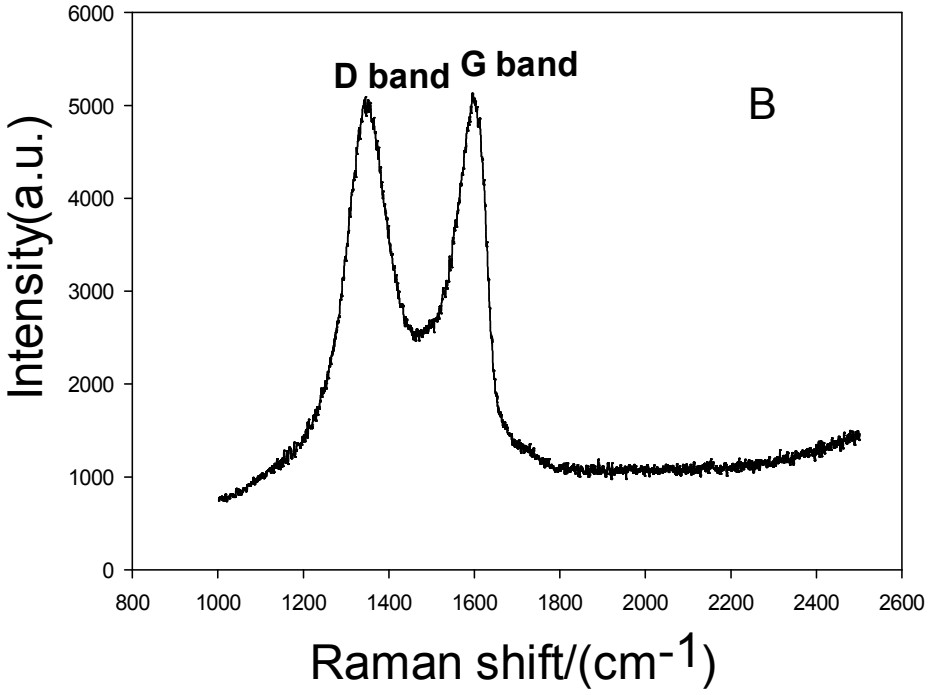

Fig. 3 XRD diffractograms of Cu_2O (A) and CuS (B)

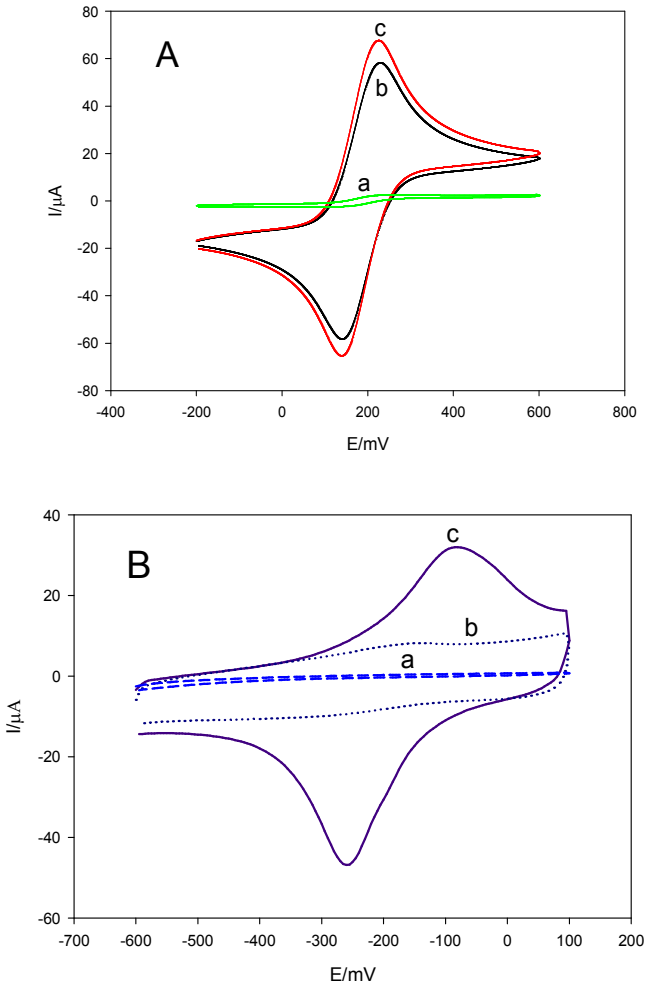

Fig. 4 (A) Cyclic voltammetry of bare GCE (a), GO/GCE (b) and RGO/GCE (c) in 5mM $K_3[Fe(CN)_6]/K_4[Fe(CN)_6]$ containing 0.1M KCl; (B) Cyclic voltammetry of the bare GCE (a), RGO/GCE (b) and CuSHNs/RGO/GCE (c) in 0.1M PBS (pH=7.0).

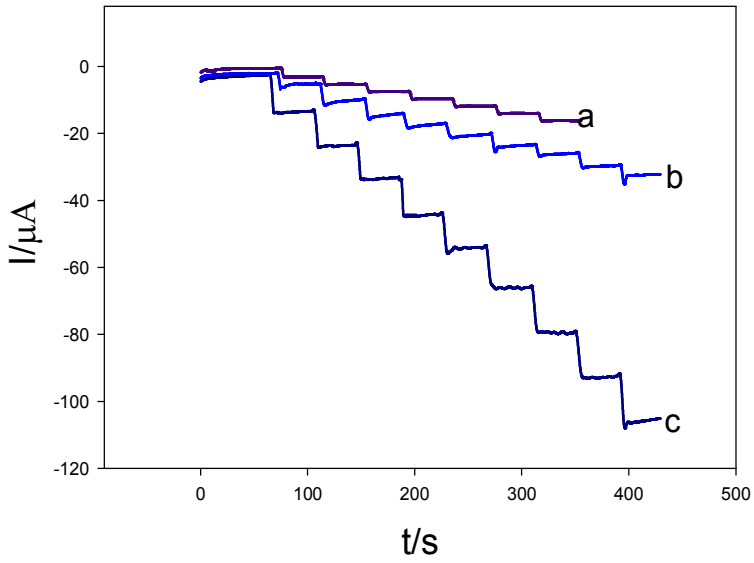

Fig. 5 Amperometric responses of the RGO/GCE (a), CuSHNs/GCE (b) and CuSHNs/RGO/GCE (c) to successive additions of 2mM H_2O_2 into 0.1M PBS (pH=7.0) at -100mV.

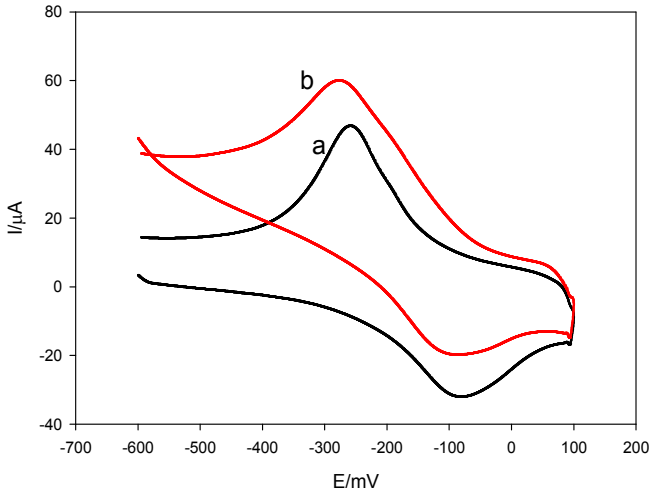

Fig. 6 CVs of CuSHNs/RGO/GCE in N_2-saturated 0.1 M PBS (pH=7.0) in the absence (a) and presence (b) of 1mM H_2O_2 at a scan rate of 100mV/s.

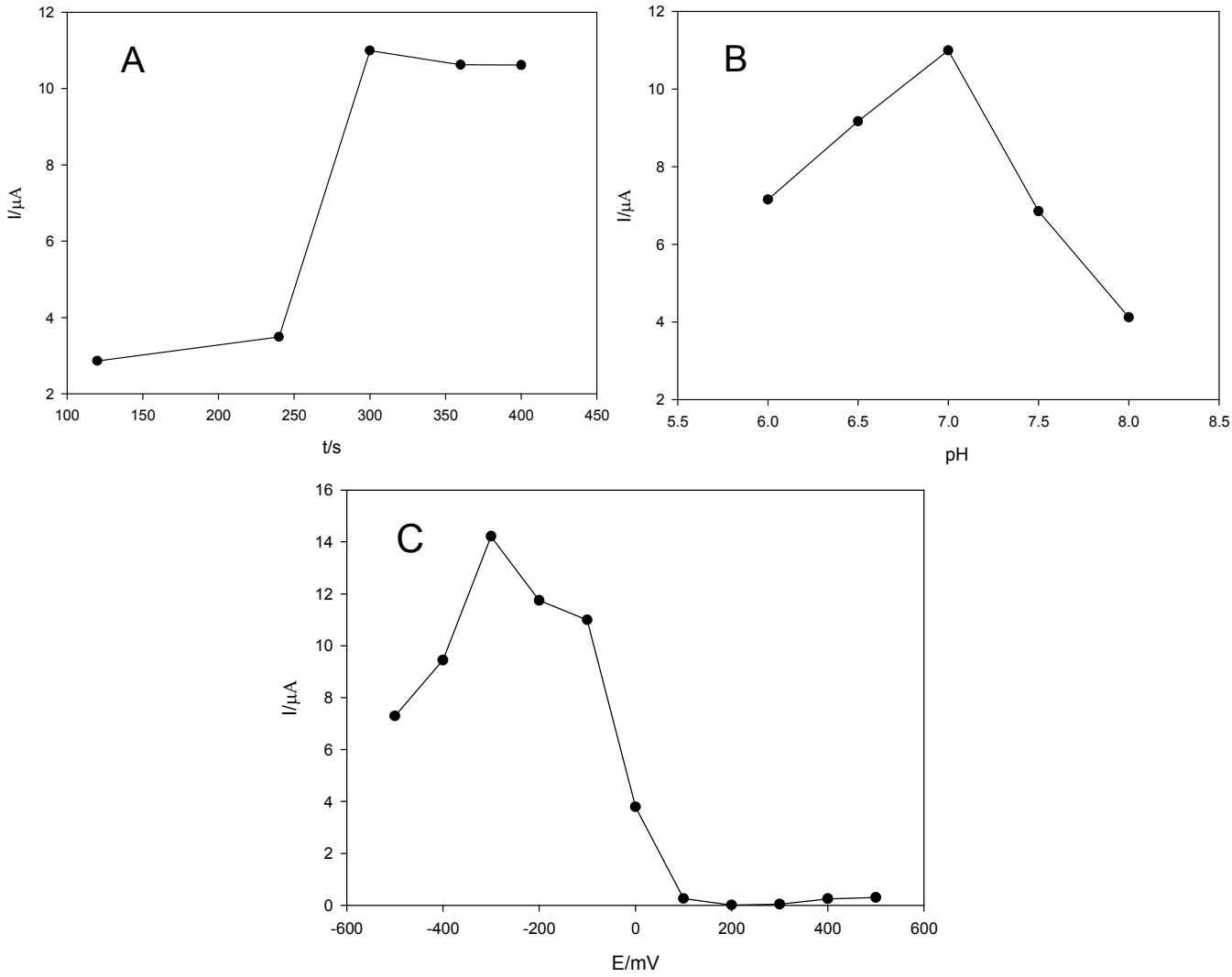

Fig. 7 Effects of the reduction time of GO (A) and pH value of PBS (B) on the amperometric responses of CuSHNs/RGO/GCE toward 2mM H_2O_2 at -100mV; effect of the applied potential (C) on the amperometric responses of CuSHNs/RGO/GCE toward 2mM H_2O_2.

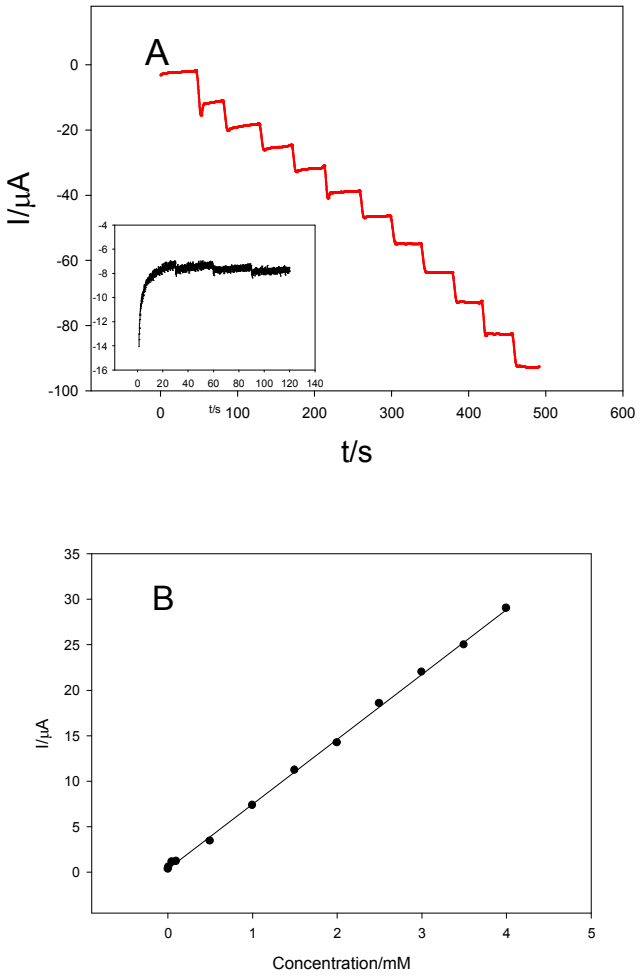

Fig. 8 (A) Amperometric responses of HCuSPs/RGO/GCE on successive injection of 1.0mM H_2O_2 into 0.1M PBS (pH=7.0) at the applied potential of -300mV (inset $[H_2O_2]$ = 0.005 mM); (B) The calibration plot of the amperometric responses versus the H_2O_2 concentration under the optimized conditions. Applied potential: -300mV.

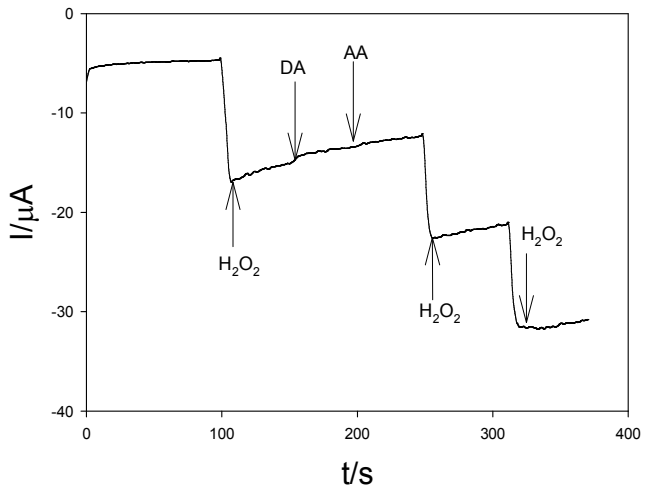

Fig.9 Amperometric responses of CuSHNs/RGO/GCE upon the successive additions of 1.3 mM H_2O_2, 1.3 mM dopamine (DA) and 1.3 mM ascorbic acid (AA) into N_2-saturated 0.1M PBS (pH=7.0) under a stirring condition. Applied potential: −300mV.